Science Advances

AAAS

advances.sciencemag.org/cgi/content/full/2/10/e1601650/DC1

Supplementary Materials for

Entropy-driven structural transition and kinetic trapping in formamidinium lead iodide perovskite

Tianran Chen, Benjamin J. Foley, Changwon Park, Craig M. Brown, Leland W. Harriger, Jooseop Lee, Jacob Ruff, Mina Yoon, Joshua J. Choi, Seung-Hun Lee

Published 21 October 2016, *Sci. Adv.* **2**, e1601650 (2016)
DOI: 10.1126/sciadv.1601650

This PDF file includes:

Tables of Atomic Parameters for the Three Structural Phases

The structural parameters refined from the BT1 data for three different phases of $FAPbI_3$ are listed in the tables below; the cubic phase (table S1), Hex-IT phase (table S2), Hex-LT (table S3).

table S1. Refined structural parameters of $FAPbI_3$ for 390 K. Positions within cubic $Pm\bar{3}m$ and occupancies per chemical unit cell (c.u.) in $FAPbI_3$ at $T = 390$ K were determined using Rietveld analysis of the neutron diffraction data shown in Fig. 1A. The lattice parameters are a = 6.3855(2) Å. Isotropic Debye-Waller factors, $\exp(-\langle u^2\rangle Q^2)$, were used where $\langle u^2\rangle = U_{iso}$ is the mean squared displacement. The Debye-Waller factors for the atoms forming FA^+ molecules were constrained to be the same. The goodness of the fit was $\chi^2 = 1.024$. $\chi^2 = \frac{1}{N}\sum_i \frac{(y_{C,i}-y_{O,i})}{\sigma^2[y_{O,i}]}$, where N is the number of data points, $y_{O,i}$ and $y_{C,i}$ are the observed and computed intensity values at $2\theta_i$, respectively. $\sigma^2[y_{O,i}] = \langle(y_{O,i} - \langle y_{O,i}\rangle)^2\rangle$.

Atom	Wyck	x	y	z	Occ	U_{iso}(Å^2)
Pb	1a	0	0	0	1	0.0428(6)
I	3d	0.5	0	0	1	0.093(1)
N	48n	0.5+0.1806 X_i	0.5+0.1806 Y_i	0.5+0.1806 Z_i	1/(24n)	0.08(2)
C	48n	0.5+0.0722 X_i	0.5+0.0722 Y_i	0.5+0.0722 Z_i	1/(48n)	=N U_{iso}
H	48n	0.5+0.2439 X_i	0.5+0.2439 Y_i	0.5+0.2439 Z_i	1/(48n)	=N U_{iso}
D1	48n	0.5+0.3191 X_i	0.5+0.3191 Y_i	0.5+0.3191 Z_i	1/(24n)	=N U_{iso}
D2	48n	0.5+0.2708 X_i	0.5+0.2708 Y_i	0.5+0.2708 Z_i	1/(24n)	=N U_{iso}

Note: the orientation of $HC(ND_2)_2^+$ is randomly distributed. X_i, Y_i and Z_i are randomly chosen and fulfills $\sqrt{X_i^2 + Y_i^2 + Z_i^2} = 1$ with i = 1, 2,…, n where n is a sufficiently large number for the isotropic model. (n=10 in our refinement)

table S2. Refined structural parameters of $FAPbI_3$ for 220 K. Positions within hexagonal $\boldsymbol{P6_3/mmc}$ and occupancies per chemical unit cell (c.u.) in $FAPbI_3$ at $\boldsymbol{T = 220}$ K were determined using Rietveld analysis of the neutron diffraction data shown in Fig. 1B. The lattice parameters are a = 8.6226(5) Å, c = 7.9458(5) Å. $\boldsymbol{\chi^2 = 1.323}$.

Atom	Wyck	x	y	z	Occ	U_{iso}(Å^2)
Pb	2a	0	0	0	1	0.059(2)
I	6h	0.83067(40)	0.16932(40)	0.25	1	0.049(1)
N1	24l	0.25362(65)	0.65483(100)	0.39236(125)	1/12	0.088(3)

N2	24l	0.38204(64)	0.67396(61)	0.13163(105)	1/12	=N1 U_{iso}
C	24l	0.38458(27)	0.67434(64)	0.29580(105)	1/12	=N1 U_{iso}
H	24l	0.50615(90)	0.69242(215)	0.35738(114)	1/12	=N1 U_{iso}
D1	24l	0.13323(101)	0.63691(249)	0.34973(161)	1/12	=N1 U_{iso}
D2	24l	0.49218(115)	0.69036(198)	0.06909(111)	1/12	=N1 U_{iso}
D3	24l	0.27049(112)	0.65735(80)	0.51922(121)	1/12	=N1 U_{iso}
D4	24l	0.27611(95)	0.65818(73)	0.05963(120)	1/12	=N1 U_{iso}

table S3. Refined structural parameters of $FAPbI_3$ for 15 K. Positions within hexagonal $\boldsymbol{P6_3/m}$ and occupancies per chemical unit cell (c.u.) in $FAPbI_3$ at $\boldsymbol{T = 15}$ K were determined using Rietveld analysis of the neutron diffraction data shown in Fig. 1C. The lattice parameters are a = 8.5070(2) Å, c = 7.9505(2) Å. $\boldsymbol{\chi^2 = 2.256}$.

Atom	Wyck	x	y	Z	Occ	U_{iso}(Å^2)
Pb	2b	0	0	0	1	0.01025(75)
I	6h	0.87344(42)	0.21250(40)	0.25	1	0.00775(61)
N1	12i	0.30380(40)	0.63940(38)	0.39349(9)	1/6	0.01336(49)
N2	12i	0.32899(41)	0.66271(38)	0.10338(1)	1/6	=N1 U_{iso}
C	12i	0.38935(13)	0.71856(17)	0.25519(17)	1/6	=N1 U_{iso}
H	12i	0.52222(44)	0.84150(56)	0.26748(56)	1/6	=N1 U_{iso}
D1	12i	0.17870(54)	0.52365(60)	0.39838(46)	1/6	=N1 U_{iso}
D2	12i	0.40754(70)	0.73540(67)	0.00444(22)	1/6	=N1 U_{iso}
D3	12i	0.36406(71)	0.69516(66)	0.50528(9)	1/6	=N1 U_{iso}
D4	12i	0.20673(57)	0.54958(57)	0.07560(37)	1/6	=N1 U_{iso}

Preferred Orientation of FA^+ Cation in Hexagonal Phase

In the hexagonal structure, the orientation of organic cations with respect to the crystal structure can be described with three Euler angles, α, β, γ as shown in fig. S1. β defines the angle between the molecular plane and the hexagonal *ab*-plane. α defines the angle between one of the hexagonal principal axis on *ab*-plane and the line of node, i.e. the intersection line between the molecular and hexagonal *ab*-plane. γ defines the angle between the C-H bond and the line of node. In the hexagonal phase, the FA^+ cations were found to have β of ~ 90^o (Fig. S1 D), indicating that the molecular plane is perpendicular

to the hexagonal *ab*-plane (or XY plane). α stays at 5° or 55° (Fig. S1 E) and γ is around 30°. Fig. 1C and 1F show the diffraction data obtained at 15 K and the refined Hex-LT structure with the *P6₃/m*.

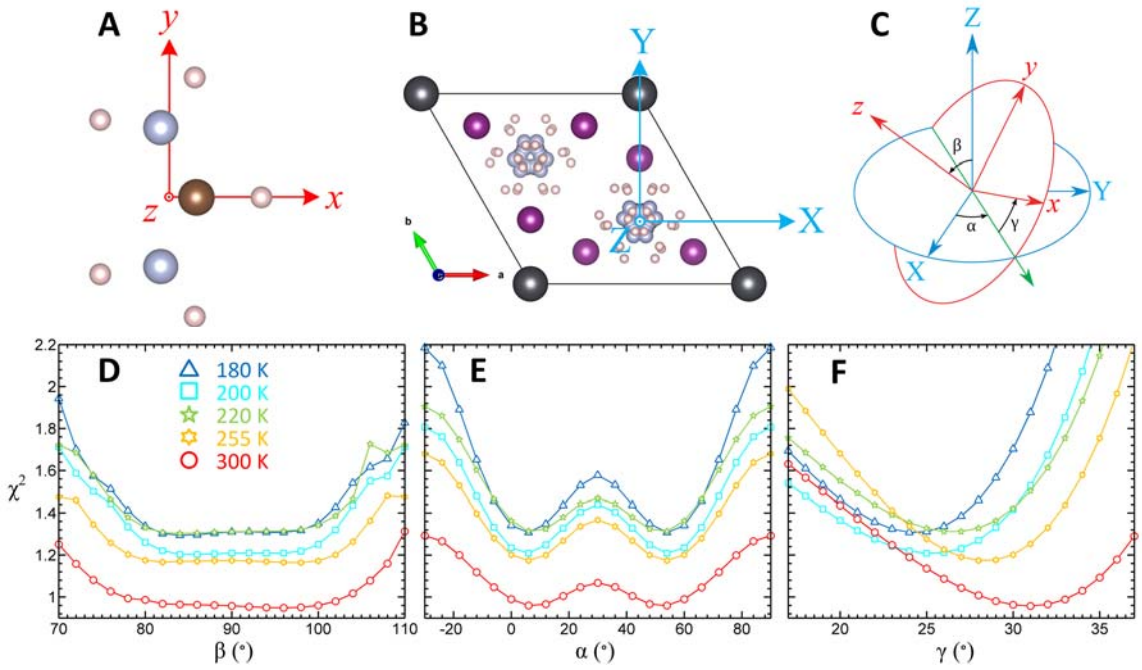

fig. S1. Orientation of FA^+ cation. (**A**) $HC(ND_2)_2^+$ cation and the molecular XYZ coordinates (red). X is along the C-H bond and Z is perpendicular to the molecular plane formed by N-C-N bonds. (**B**) The relative orientation of molecules with respect to the crystal structure XYZ coordinates (blue). (**C**) Euler angles, α, β and γ, that determine the relative orientation of the molecular (red) and crystal (blue) coordinate systems. (**D**), (**E**), (**F**) show the goodness of the refinement as a function of Euler angles at several different temperatures in the *P6₃/mmc* phase.

Synchrotron X-ray Diffraction Measurements

Our neutron diffraction results at 220 K (Fig. 1B and table S2) indicate that the intermediate hexagonal structure has the unit vectors of (a_h, b_h, c_h) that are related to the cubic unit vectors (a_c, b_c, c_c) in the following way: $a_h = a_c - b_c$, $b_h = b_c - c_c$, and $c_h = \frac{2}{3}(a_c + b_c + c_c)$. The shrinking of the unit cell along the c_h direction is surprising because in the cubic phase along the cubic <111> direction three different hexagonal planes appear in an ABC sequence (see fig. S2). $c_h = \frac{2}{3}(111)$ means that in the hexagonal phase there are only two types of hexagonal planes in the new unit cell in an ABA sequence (see fig. S2). If the Bragg peaks of the 220K data were to be indexed while maintaining the ABC sequence, the c-axis of the new hexagonal unit cell has to be $c_h' = 2(a_c + b_c + c_c)$, as shown in the left panel of Fig. S2. In that case, however, there should be more peaks that are absent in our experimental data (see the inset of Fig. 1B). To validate this reflection condition, we have also performed synchrotron X-ray diffraction measurements and indeed found that both neutron and X-ray diffraction results indicate that the hexagonal structure has $c_h = \frac{2}{3}(a_c + b_c + c_c)$.

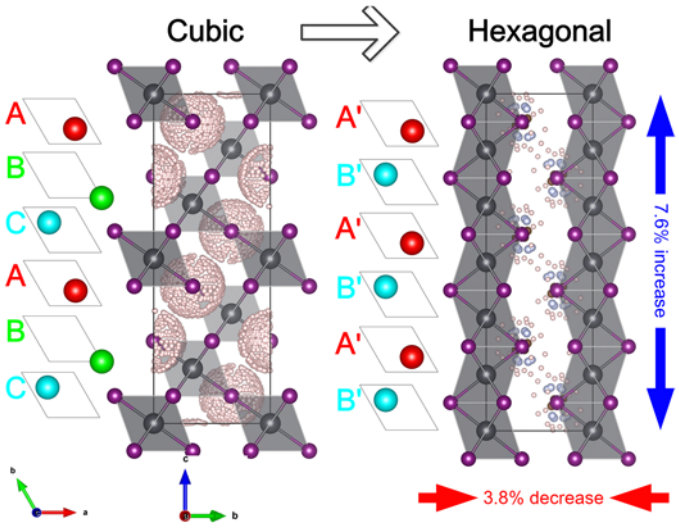

fig. S2. Refined crystal structure. (**A**) The cubic structure has an ABC stacking sequence in which the atomic locations in the $(111)_c$ plane alternate among ABC configurations. (**B**) The intermediate hexagonal phase structure shows a AB stacking sequence, resulting in shrinking of unit cell along $c_h = \frac{2}{3}(a_c + b_c + c_c)$. Red, green and cyan spheres represent the positions of organic cations in the $(111)_c$ or $(001)_h$ plane.

Synchrotron powder diffraction measurements were performed at the A2 beam line at the Cornell High Energy Synchrotron Source (CHESS). Diffraction patterns were collected with wavelength 0.5407 Å using a two-dimensional pixel array detector. The sample was cooled down to 220 K using a closed cycle refrigerator. The total exposure time was about 8 hours.

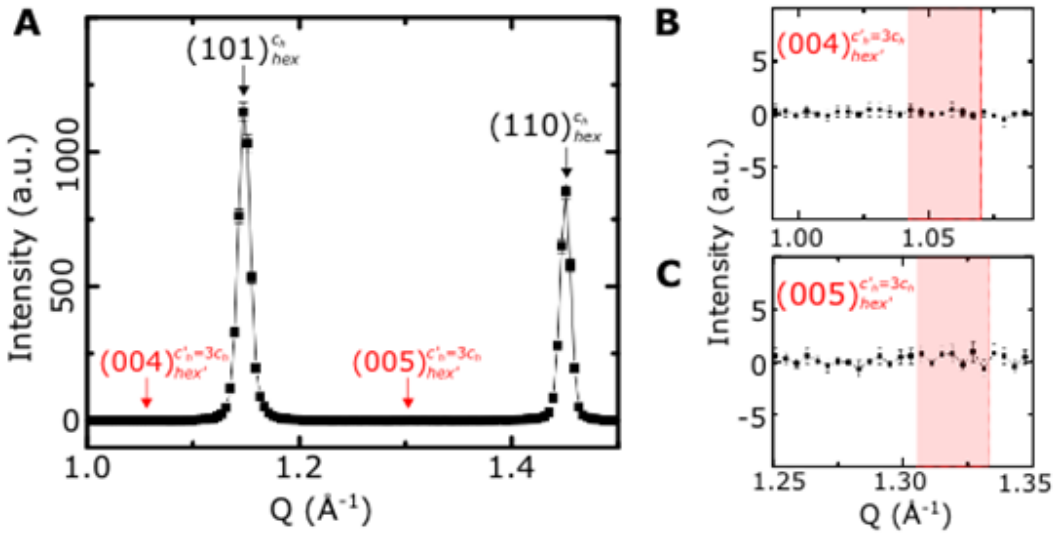

fig. S3. **Synchrotron x-ray powder diffraction data for $FAPbI_3$.** (**A**) The diffraction pattern was measured at 220 K and was obtained after subtracting the air scattering background that was fitted to a smooth polynomial function. The pink shaded areas in (**B**) and (**C**) indicate the region where Q = $(004)^{c_h'=3c_h}_{hex'}$ and $(005)^{c_h'=3c_h}_{hex'}$ peaks of the enlarged hexagonal structure with $c_h' = 2(a_c + b_c + c_c)$ are expected.

Figure S3A shows the diffraction data obtained at 220 K. The two strong peaks can be indexed by a hexagonal structure with *P6₃/mmc* space group and the unit vectors of (a_h, b_h, c_h). If the Bragg peaks of the 220K data were to be indexed while maintaining the ABC sequence as in the cubic phase, the c-axis of the new hexagonal unit cell has to be $c_h' = 2(a_c + b_c + c_c)$. In that case, however, there should be more peaks in the Q-range covered by our measurements such as Q = $(004)^{c_h'=3c_h}_{hex'}$ and $(005)^{c_h'=3c_h}_{hex'}$ shown in red in the fig. S3 (A), (B) and (C). The absence of these peaks confirms the reflection condition obtained from our neutron data and that the hexagonal structure has $c_h = \frac{2}{3}(a_c + b_c + c_c)$.

Confirmation of Thermal Equilibrium during Neutron Measurement

To ensure the thermal equilibrium before taking the elastic neutron data at SPINS, we waited 16.6 minutes after temperature was changed to a set temperature. To check for the thermal equilibrium, we followed the peak positions of the $(1,1,1)_c$, $(0,2,0)_h$, $(1,1,1)_h$ nuclear Bragg peaks during warming and cooling shown in fig. S4. The decreasing in Q with increased temperature is due to thermal lattice expansion. The fact that the Q values of the peaks during warming and cooling processes overlap with each other confirms the thermal equilibrium of the sample during the measurements. The observed thermal hysteresis is not due to experimental artifacts but is an intrinsic property of the system.

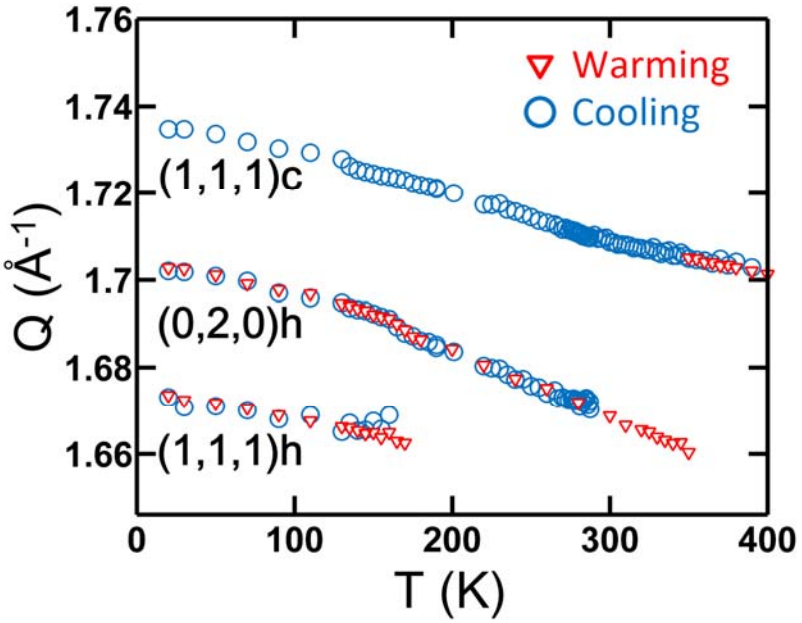

fig. S4. Check for thermal equilibrium during elastic neutron scattering measurements. During the measurements taking the data shown in Fig. 2, the temperature of sample was equilibrated with a wait time of 16.6 minutes at each set temperature. The data shown in Fig. 2 was fitted to Gaussians to obtain the peak positions shown in this figure. The red triangles (blue circles) represent the peak positions of the three peaks obtained during the warming (cooling) process.

Kinetic Trapping of the Cubic Structure by Thermal Quenching

We have performed a rapid quenching experiment in which the sample was heated to 400 K and cooled to 200 K over ~80 minutes. No phase transition was detected and the whole system remained cubic (See Fig. 3A). The sample was monitored for 1 hour at 200 K and still no phase transition was observed. Upon further cooling to 8.2 K and monitoring for 7 additional hours, the system remains in the cubic phase. (See fig. S5). This confirms the system being kinetically trapped in the cubic state in a rapid temperature quenching condition to below ~270 K.

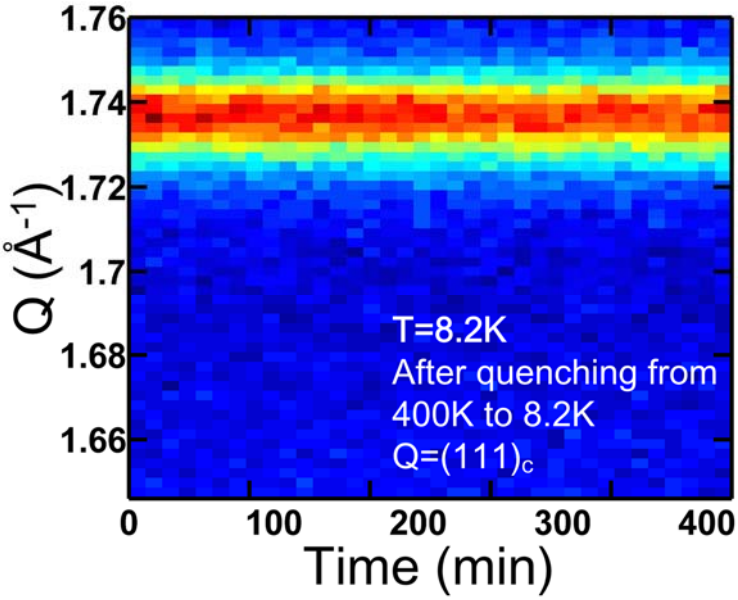

fig. S5. Temporal monitoring of the stability of the cubic phase at 8.2 K after thermal quenching. The nuclear $(111)_c$ Bragg peak of the cubic structure of $FAPbI_3$ was measured over 400 minutes at 8.2 K after quenching from 400 K.

Details on Density Functional Theory Calculations

Our ab initio density functional theory calculations (DFT) use projector augmented wave (*26*) to describe the core electrons and the generalized gradient approximation with the Perdew-Burke-Ernzerhof functional (*27*), as implemented in VASP (Vienna Ab initio Simulation Package) code (*28*). The kinetic energy cutoff for the plane-wave basis is set to 400 eV. 4×4×4 *k*-points are sampled through Monkhorst-Pack scheme (*21*) for cubic unit cell and equivalent and denser sampling was used for supercell structures. All the structures

are fully relaxed until the force on each atom is less than 0.02 eV/Å. We obtain the lattice constants of a = 8.983 (8.6226) Å, c = 8.206 (7.9458) Å for the LT-hexagonal phase and a = 6.493 (6.3855) Å for the cubic phase by Birch-Murnaghan fitting (*29*, *30*). These values are in good agreement with experimental values listed in the parenthesis. For a given optimized lattice constant, FA^+ cation is fully relaxed. However, since the optimization is performed at zero temperature, FA^+ cations remain frozen at the local minimum near the assigned orientation. Such a frozen FA^+ cation can locally break cubic symmetry, thus the cubic phase energy has some ambiguity in our calculation settings. However, we confirm that for any relaxed configurations that we considered the energy of the cubic phase is always higher than the hexagonal phase, identifying the hexagonal phase as the most favorable configuration at zero temperature.

In order to obtain the potential energy landscape of the transition pathway, we performed constrained structure optimization for each initial transition states generated from the interpolation between cubic and hexagonal phase. We define a reaction coordinate which possess a monotonically increasing (or decreasing) Cartesian coordinate for a chosen pathway. Generally, the energetically favorable transition pathway consists of transition states with local energy minima in the configuration space except one direction (reaction coordinate). Thus, we adopt a constrained relaxation scheme to fully relax initial transition states except the reaction coordinate. We assume that the proposed transition states are not so far from the minimum energy pathway, thus expect that such a constrained relaxation scheme always drives the structure to the energetically favorable transition pathway.